Numerical Modeling of Topographic Influences on Shallow Front Formation and Evolution: Quasi-Stationary Coastal Front

CHING-YUANG HUANG[1]

ABSTRACT

A two-dimensional mesoscale numerical model is used to investigate topographic influences on shallow front formation and evolution. The shallow front is idealized as a coastal front near the southeastern China coast, with the downstream topographic features including the Taiwan Strait, the Taiwan Island and the Central Mountain Range (CMR). Shallow frontogenesis near the coast occurs as a direct result of differential heating in the boundary layer for near-surface onshore ambient flow. The idealized shallow coastal front shows similar thermal structures with the lower part of Mei-Yu fronts stagnating over the southeastern China coast, indicating that differential heating for the former similarly plays the role of geostrophic deformation in frontogenesis for the latter. Although the packed frontal isentropes tend to reside over the China coast, the frontal leading updraft may advect offshore as the shear of the upper-level offshore ambient flow is present. The associated cloud band hence is not necessarily confined near the China coast. Based on the numerical control experiments, cloud development in response to the interaction processes among the moving frontal updraft, the developed land breeze over the island and the CMR is discussed.

1. INTRODUCTION

Near-coast fronts are usually shallow as compared to deep fronts inland (*e.g.*, Chen *et al.*, 1989). The shallowness of the near-coast front may be related to effects of air mass modification as the inland front migrates offshore or even stagnates near the coastal region. Due to the complexity of the frontal structure, modeling the influence of a near-coast shallow front on the downstream environment has great challenges. No cold-front theory (*e.g.*, Hoskins and Bretherton, 1972) is found to be suitable for rendering an initial frontal field that could approximate the shallowness and intensity of the near-coast front

---

[1] Institute of Atmospheric Physics, National Central University, Chung-Li, Taiwan 32054, R.O.C.

of mesoscale. The difficulties in the initialization of a mesoscale model for the near-coast front also stem from the fact that shallow fronts such as Mei-Yu fronts are evidence of the processes of geostrophic deformation between the anticyclonic high over Northern China and the subtropical high over the Pacific Ocean (*e.g.*, Chen *et al.*, 1989). It is not an easy task for a mesoscale model to account for effects of such large-scale flow deformation in order to produce a localized shallow front.

In addition to the process of geostrophic deformation, there are other processes that could also result in frontogenesis. Differential heating in the boundary layer has been known to play the role of geostrophic deformation in packing the isentropes in large-scale frontogenesis (Hoskins and Bretherton, 1972; Bosart, 1975). Observations used to indicate that intense coastal frontogenesis due to the differential heating mechanism could cause highly deformational flow near the coast for uniform onshore ambient flow conditions (Bosart, 1981). Three-dimensional numerical simulations also showed that the Carolina coastal frontogenesis resulted from such mechanism, with mesoscale convective systems over the surface front (Huang and Raman, 1992).

In this study, we will rely on a mesoscale model to generate a coastal shallow front through the differential heating mechanism. We hope to use numerical control experiments to sketch the characteristic features of the shallow front and the frontal cloud development in the vicinity of the southeastern China coast. In particular, effects of local terrain on the development of an upstream frontal cloud band will be investigated. This numerical investigation does not aim at providing an explanation of near-coast Mei-Yu frontogeneses (for such cases see Chen and Hui, 1990), but has focused on the interaction processes between a quasi-stationary near-coast shallow front and the downstream complex topography which consists of the Taiwan Strait and high mountains over Taiwan Island. It is mainly concerned with how the Taiwan topography influences the downstream propagation of the frontal cloud band. We will introduce the mesoscale numerical model in Section 2 followed by the presentation and discussions of the numerical results. Finally, a brief conclusion will be given.

2. THE NUMERICAL MODEL AND CASE EXPERIMENTS

2.1 The Numerical Model

The present mesoscale numerical model is the same as the one in Huang and Raman (1992). The model is hydrostatic and anelastic in a terrain-following coordinate system. The model physics includes cloud microphysics that basically follows Kessler's formulations. To account for horizontal advection, a modified version of Warming-Kutler-Lomax (WKL) advection scheme is used. This modified scheme performs closely to the fourth-order leapfrog scheme, but saves considerable computer memory because of its two-time-level feature (see Huang and Raman, 1991b). In the vertical, the second-order Crowley advection scheme is employed to reduce the complexity of the finite-difference formulation in the stretched grid mesh.

A turbulence closure scheme based on two prognostic equations, one for the turbulent kinetic energy (TKE) and the other for turbulence energy dissipation (ε), is incorporated with the level 2.5 formulation of Mellor and Yamada to determine eddy diffusivity (see Huang and Raman, 1991a). Since coastal frontal circulations are essentially driven by boundary layer effects, a turbulence closure scheme including comprehensive physics is helpful for

resolving the boundary layer structure. In consideration of rigorous turbulent transfer in case simulations, a time-implicit scheme is used to account for all vertical diffusion terms of the model equations for eliminating numerical instability.

2.2 The Case Experiments

We will limit ourselves to 2-D cases since our primary objectives are to figure out how the fronts respond to the effects of the underlying topography parallel to the frontal axis and to investigate the relative importance of the frontal dynamics and topographic effects. Two-dimensionality, although greatly simplifying the real conditions, facilitates our dynamic understanding of the responses. It also enables a use of finer horizontal and vertical grid resolutions so that the updrafts of dominant scale are not misrepresented due to the insufficient model resolution.

In this study, we concentrate on the coastal frontal circulation where a near-surface onshore ambient flow appears to be a pre-condition for its formation (Bosart, 1975; Huang and Raman, 1992). Four case experiments were conducted in this study and are described in Table 1. In Case 1, the initial flow is barotropic and onshore, thus favorable for stationarity

---

Table 1. A description of two-dimensional case experiments* in this study.

Case No.	Descriptions of Experimental Parameters
1	$U_g = -4$ m/s, No vertical shear, RH = 50 %, CMR
2	$U_g = -4$ m/s, $\partial U_g/\partial z = 0.004$ s^{-1}, RH = 80 %, CMR
3	$U_g = -4$ m/s, $\partial U_g/\partial z = 0.004$ s^{-1}, RH = 50 %, CMR
4	$U_g = -4$ m/s, $\partial U_g/\partial z = 0.004$ s^{-1}, RH = 50 %, CMR removed

*All cases employ the Coriolis parameter f at a latitude of 25^0, stability stratification N ~ 0.01 s^{-1}, and a coastal SST gradient equal to 15 ^{0}C/10 km with $\Delta x = 5$ km and $\Delta t = 30$ s for 36 hour simulation time. The initial potential temperature has a constant vertical gradient of 4 ^{0}C km^{-1}. The Central Mountain Range (CMR) is idealized as a Gaussian distribution with the central height of 3 km.

---

of the front. Case 2 includes the wind shear where the flow becomes offshore above 1 km. Case 3 is identical to Case 2, except with a uniform relative humidity reduced to 50% from 80%. These three cases include the Central Mountain Range (CMR) which has been idealized as a Gaussian barrier with the central height of 3 km. The CMR is removed in Case 4 for comparison with Case 3. There are 150 horizontal grids in the model with a uniform grid interval of 5 km. The center of the CMR lies on grid 96 with the western and eastern coastlines on grids 80 and 104, respectively. The southeastern China coastline is on grid 40,

about 200 km west of the western Taiwan coastline. In the vertical, there are 36 grids with a constant interval of 250 m below 5 km, above which spacing is 500 m up to 12 km height.

The model initialization follows our previous studies and the details can be found in Huang and Raman (1992). The CMR is gradually lifted to its final height within the first simulation hour. Initially, the flow is assumed to be horizontally homogeneous and is heated up by the warmer sea surface water. For simplicity, initial relative humidity (RH) is also assumed to be constant over the model domain (see Table 1). Initial ground temperature is set to 10°C; that is relatively cold in contrast to the sea surface temperature (SST) of 25°C. Zero sensible heat flux is assumed over ground, thus the flow possesses a neutral surface layer. Over water, air temperature is modified according to surface layer similarity theory. Total numerical simulation time is 36 hours with an integration time step of 30 s. Sea surface temperatures are unmodified during the numerical simulation time. The simulated ambient environment is at a moderately stable condition with a constant vertical potential temperature gradient of 4°C km^{-1}. Radiation conditions are used at the lateral and upper boundaries for allowing the outward propagation of internal gravity waves (for details, see Huang and Raman, 1991b, 1992).

The coastal baroclinicity imposed in the simulated cases has a sea-surface temperature (SST) variation of 15°C within a distance of 10 km to the ground. This large magnitude of surface temperature gradient is not pertinent to real Mei-Yu cases. Indeed, the initial condition of SST is closer to the winter cases in which intense cold air masses stagnate over China. In reality, the southeastern China coast in late Spring has surface air-temperature variations around 15-20°C and the SST around 22-26°C depending on the geometric position of the China coast (see Tang and Chen, 1990). Due to the surrounding ocean, Taiwan indeed has higher surface air temperature than the southeastern China coast. The initial settings imposed in the model are thus about two times stronger than the observed. This strong coastal baroclinicity is used for introducing an intense shallow front. After integration, the initial condition will be gradually adjusted in response to the boundary layer forcing. A considerable reduction on the temperature gradient between the sea and land does not significantly change the circulation pattern but weakens the frontal intensity and the associated cloud development.

3. THE MODEL RESULTS

It should be noted that no horizontal air-temperature variation exists in the initial field for the four cases. The atmospheric baroclinicity is induced solely by the coastal oceanic baroclinicity as the heat and moisture transfers are differentially transported upward over the coastal region. As the atmospheric baroclinicity is prominently induced near the coast, mesoscale coastal circulation would develop. Figure 1 shows the time evolutions of maximum and minimum vertical wind velocities in the model domain during the 36 h integration time for the four cases. After the initial adjustment period of terrain lifting (the first 1-2 hours), the circulation system for the shear case (Case 3) develops much slower than that for Case 2 with higher RH. For onshore flow, the nonshear case (Case 1) exhibits stronger vertical motions than the shear case, particularly for the downward motion. Case 4 with removal of the CMR, has in a general trend the weakest system development among all the cases, except at the later stage over 30 h. For the other case with the CMR and higher moisture contents, the system is more subject to oscillations that are believed to be caused by gravity wave propagation excited by the convective clouds. The presence of the constant shear of
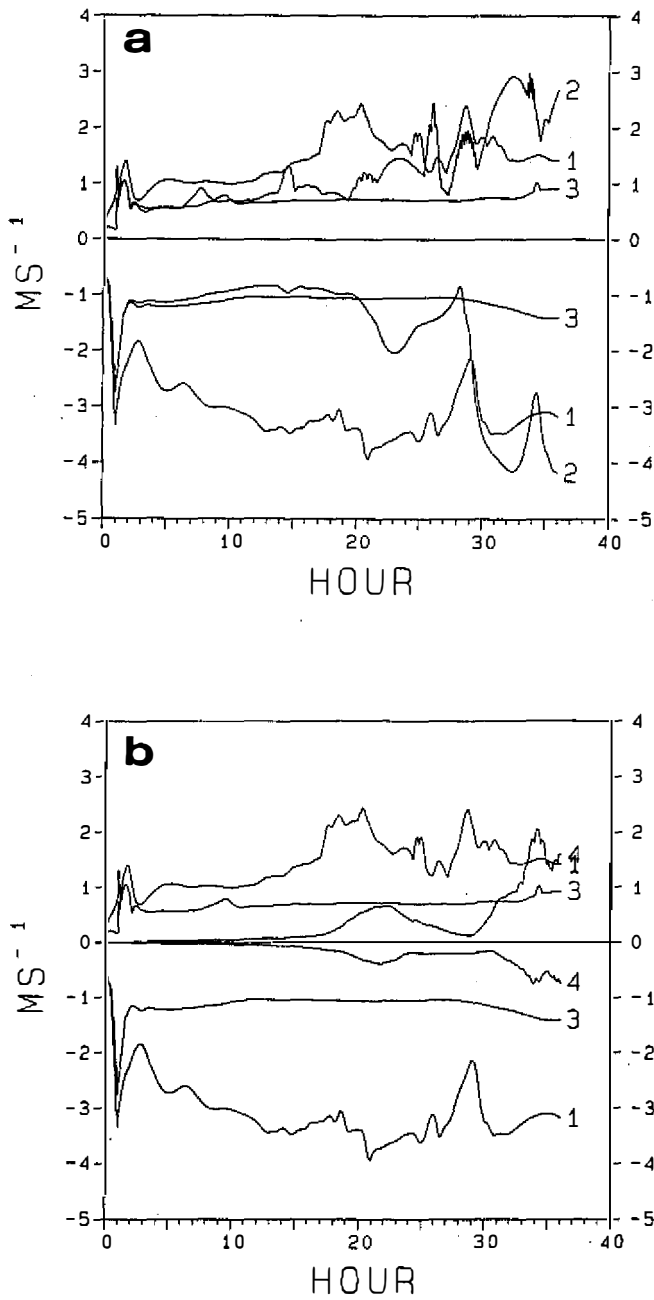
Fig. 1. Time evolutions of maximum and minimum vertical velocities in the model domain. (a) Cases 1, 2 and 3; (b) Cases 1, 3 and 4.

0.004 s^{-1} tends to deactivate the wave excitement in a relatively dry environment so that the flow seems to reach quasi-steady state for Case 3.

The mesoscale circulations induced by the topographical effects at 12 h are shown in Figure 2 for Cases 1 and 2 (at this time, the results of the other two cases are similar also). As can be seen, a coastal front is present up to a level of 1.3 km near the China coastline (grid 40). Over the Taiwan Island, land breezes develop to a level of about 1 km at the two sides of the CMR. It can also be found that the eastern land breeze somewhat deforms in the nonshear case (Case 1) as compared to the shear case (Case 2). In the shear case, the upper-level offshore flow tends to support the eastern breeze development. Due to the pushing of onshore flow at whole levels, the land breeze for the nonshear case is suppressed at the upstream (eastern) side and is somewhat stronger at the downstream (western) side. Mountain waves are much steeper for the nonshear case but are significantly attenuated for the shear case. Therefore, the shear structure above 1 km (where the flow becomes reversed) with a northward vorticity vector tends to suppress the vertical displacement of disturbances.

For a better exhibit of the mountain flow, the low-level island circulation is presented in Figure 3. Deep mountain waves are found to appear over the western CMR slope for the uniform ambient onshore (easterly) flow (Case 1). The shear of ambient offshore (westerly) flow, however, produces small wave amplitudes for Case 2. Major clouds form at the upstream (eastern) slope of the CMR for both Cases 1 and 2. As seen, the eastern land breeze for Case 1 has deformed and causes higher and stronger cloud development. Land breezes at the other (western) side for both the cases are seen to migrate offshore and cause little cloud formation. For Case 2, there is an updraft over the eastern slope of the CMR, confronting the downdraft near the top of the CMR. This convergence results in more level isentropes. For both the cases, the near-surface flow is completely blocked upstream of the mountain at the penetrative depth of the land breeze and thus is forced upward there. Consequently, the breeze updraft produces a cloud-core formation away from the mountain region.

The mesoscale circulation develops further at 24 h (Figure 4). As can be seen, the temperature contrast across the front is about 6-7°C for all the four cases. Also, the potential temperature field over the front has been greatly modified by the intruded warmer maritime flow. Since the ambient wind for the three shear cases becomes offshore above 1 km, the inland moisture tongue is not very prominent at higher levels. For a uniform onshore ambient flow, the moisture tongue over the front can have a larger inland penetrative depth, depending on the magnitude of the ambient wind speed. Thus, no large major clouds are produced over the inland regions for the four cases. At the island region, major cloud formation remains well formed at the upstream slope for the nonshear case (Case 1), but the eastern deformed land breeze completely diminishes at this time. The CMR tends to interrupt a downstream propagation of the cloud originating from the upstream side. For the shear case (Case 2) with higher RH, the cloud east of the mountain has propagated further offshore due to the mid-level offshore (westerly) flow. Over the Taiwan Strait, there are newly developed clouds extending from the upper branch of the western land breeze to the top of the China coastal front. The MBL height for the nonshear case is higher than that for the shear case, since the weaker flow in the MBL for the latter has weaker turbulent flux transfer. It should be noted that the low-level coastal front is quasi-stationary for all the cases.

The cloudy regions over the Taiwan Strait are separated for the shear case with less RH (Case 3), with one east of the coastal front and the other west of the western Taiwan land breeze front. This indicates the availability of the upper-level ambient moisture to be important for the formation of a big cloud as the two frontal updrafts begin to merge or
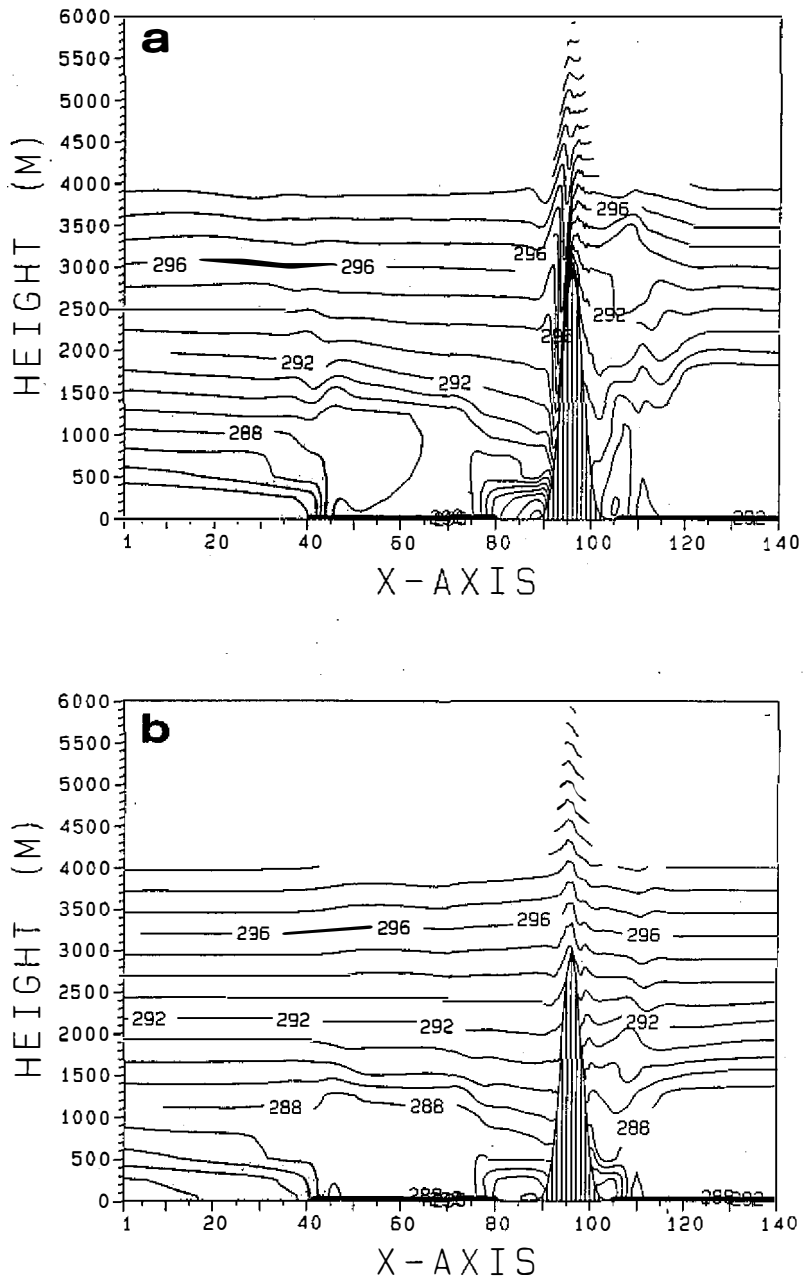
Fig. 2. The numerical results at 12 h. (a) Case 1 (with uniform onshore flow) and (b) Case 2 (with the shear). Solid lines are for potential temperature with a contour interval of 1°C. The China coastline lies on grid 40 and the Taiwan island on grids 80-104. Horizontal grid intervals are 5 km uniformly.
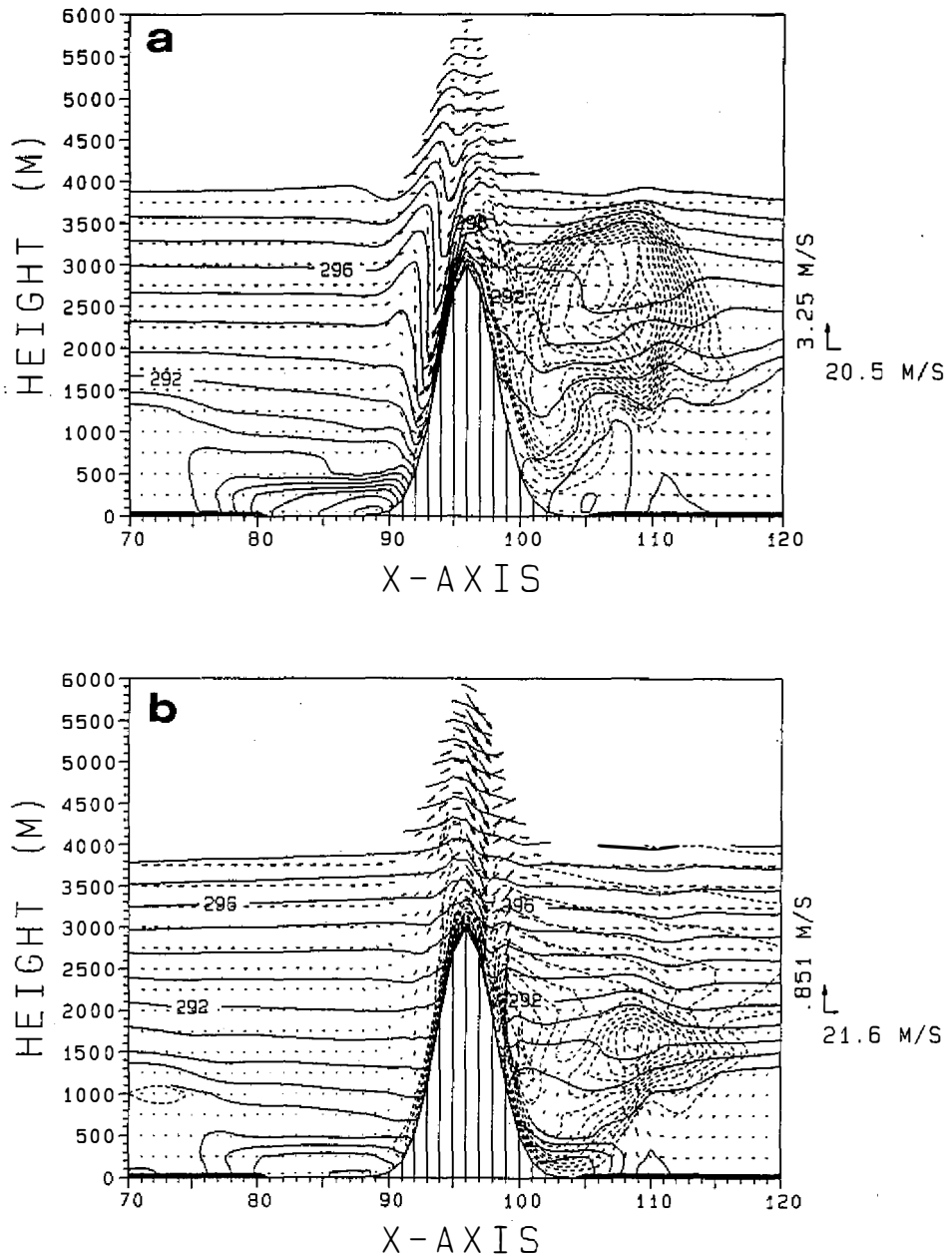
Fig. 3. Selected mountain flow regimes at 12 h. (a) Case 1 and (b) Case 2. Maximum wind vectors are plotted on the right of the panel for reference. Solid lines are for potential temperature with a contour interval of 1°C. The three contour indices (minimum, maximum, interval) in units of 0.01 g kg^{-1} for cloud water (dashed lines) are (5, 70, 5) in (a) and (5, 60, 5) in (b).
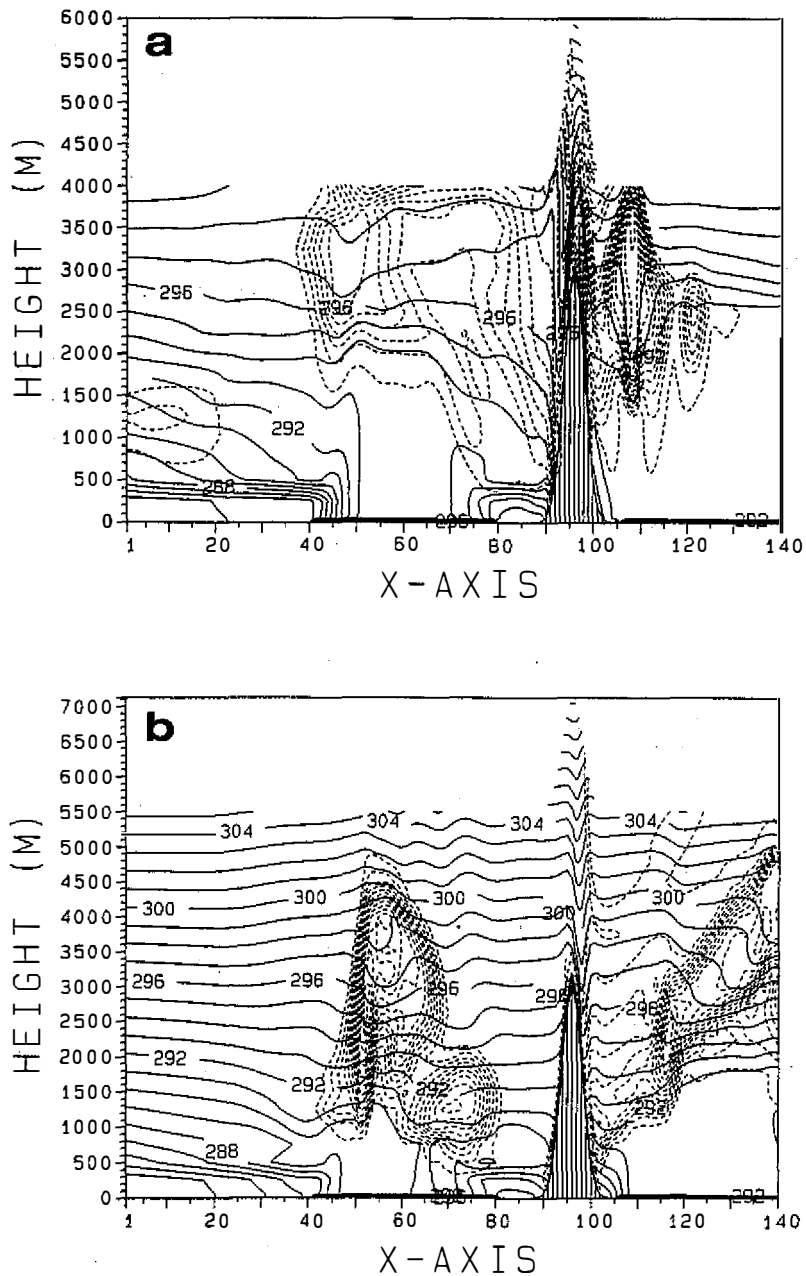
Fig. 4. The numerical results at 24 h. (a) Case 1; (b) Case 2; (c) Case 3 and (d) Case 4. The three contour indices (minimum, maximum, interval) in units of 0.01 g kg^{-1} for cloud water (dashed lines) are (5, 95, 5) in (a), (5, 65, 5) in (b), (5, 55, 5) in (c) and (5, 70, 5) in (d).
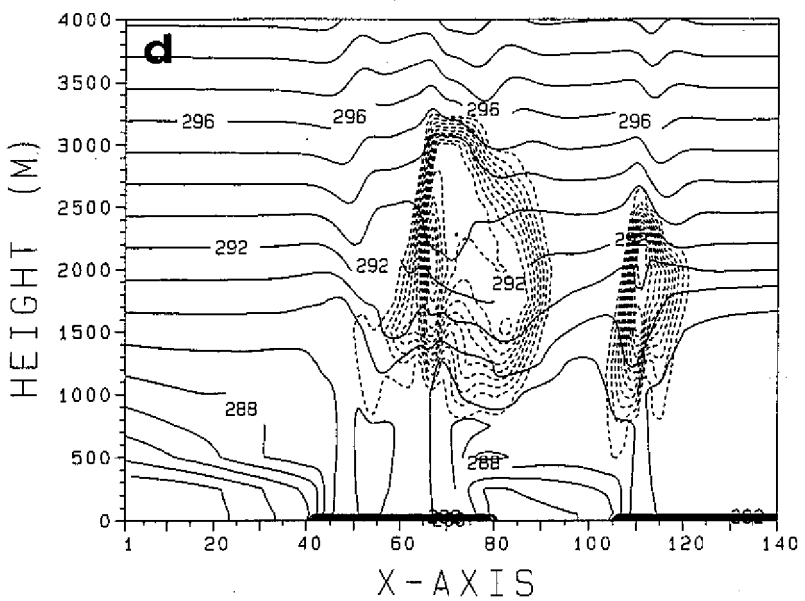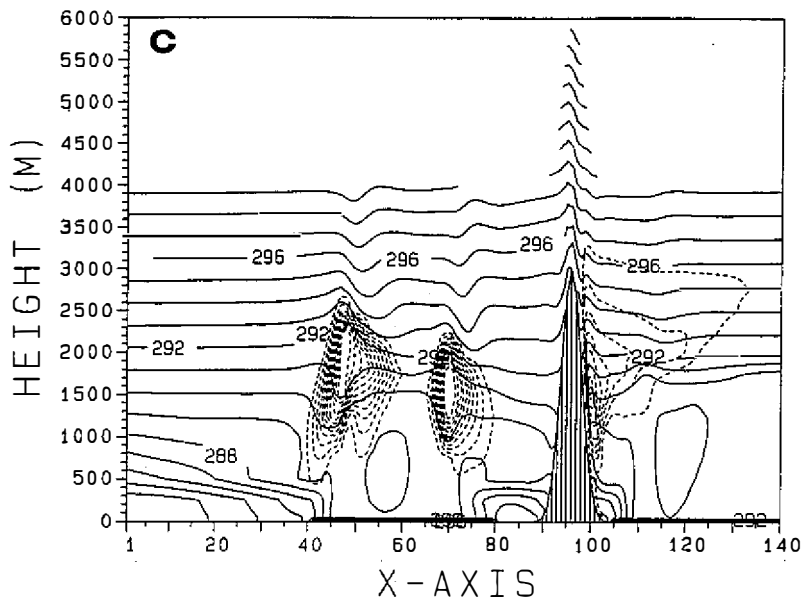
Fig. 4. (Continued.)

interact with each other. Without the mountain, this big cloud moves further inland of the western Taiwan coast as seen in Figure 4d. Since land breezes develop at both sides of the island, two major clouds form but are rather shallow in Case 4. Due to the island width (about 120 km), the two shallow clouds are unable to merge and overcast the whole island at 24 h.

The dynamic features of the MBL cloud formation should be discussed further. Figure 5 shows the updraft and cloud distributions for Cases 2 and 3 over the Taiwan Strait. As can been seen, the major coastal updraft appears on grids 51 to 53, which is about 60 km distant from the China coastline (grid 40). Although the lowest part of the coastal front remains near-stationary because of the onshore forcing of the ambient flow, the frontal updraft is able to move offshore for the shear case. In contrast, the coastal frontal updraft moves less offshore for the shear case with less RH. Since the upper-level moisture contents are greater for Case 2, the clouds east of the China coast develop much higher (up to 5 km) than for Case 3 and the cloud base west of the western land breeze is lower due to the influence of the frontal cloud on the land breeze development. An outflow jet of the shear flow appears near the top of the frontal updraft and penetrates eastward and downward into the cloud over the leading edge of the land breeze. This feeding flow enhances the breeze circulation and leads to a further offshore (westward) developing breeze updraft as compared to Case 3. Hence, the land breeze penetration is influenced by the advection of the coastal frontal cloud band, despite the fact that the water fetch is about 200 km in width.

For detailed comparisons between the results of Cases 2 and 3, the mountain flow regime is further analyzed and their results at 24 h are shown in Figure 6. For the moist case, the mountain waves are stronger than for the dry case; for example, the downdraft intensity has increased to 1.85 m s^{-1} from 1.05 m s^{-1}. Also, a thin cloud layer is present over the CMR only for the moist case as seen in Figure 3b. As the mid-level RH increases, the convergence induced by the shear flow and weak onshore flow east of the land breeze results in a second but more intense cloud over the oceanic region. This cloud is transient and propagates further offshore with time. For the dry case, the land breeze shows very light cloud over water. At the eastern side of the CMR, low-level orographic clouds are produced in both the cases. The cloud formation is caused by the updraft originating from the flow over the breeze recirculation zone at a height of about 500 m. At the western side of the CMR, both the cases exhibit considerable blocking at low levels. This is consistent with theoretical prediction, since the Froude number (defined by U/Nh, where h is the mountain height) for the flow is much less than unity.

As the circulation development proceeds to 36 h, the cloud and potential temperature fields exhibit appreciably different features (Figure 7). It is interesting to see that for the dry shear case (Case 3) the separated clouds have merged at 36 h and reside over the Taiwan Strait and the western coast of the island, while in the moist case most of the clouds have moved to stay over the land breeze zone and the CMR. This is because the leading frontal updraft moves at a faster speed for the moist case and indeed has merged into the downstream breeze (Figure 7a). For the dry case, the upper part of the frontal updraft is somewhat distant from the breeze and therefore must tilt toward the breeze in order to compensate for the upper-level outflow divergence of the breeze updraft (Figure 7b).

4. DISCUSSIONS

The mesoscale circulations presented in this study are essentially driven by the topographical effects. For the formation of the coastal front, the main mechanism is the frontogenesis of differential diabatic heating in onshore ambient flow conditions as discussed
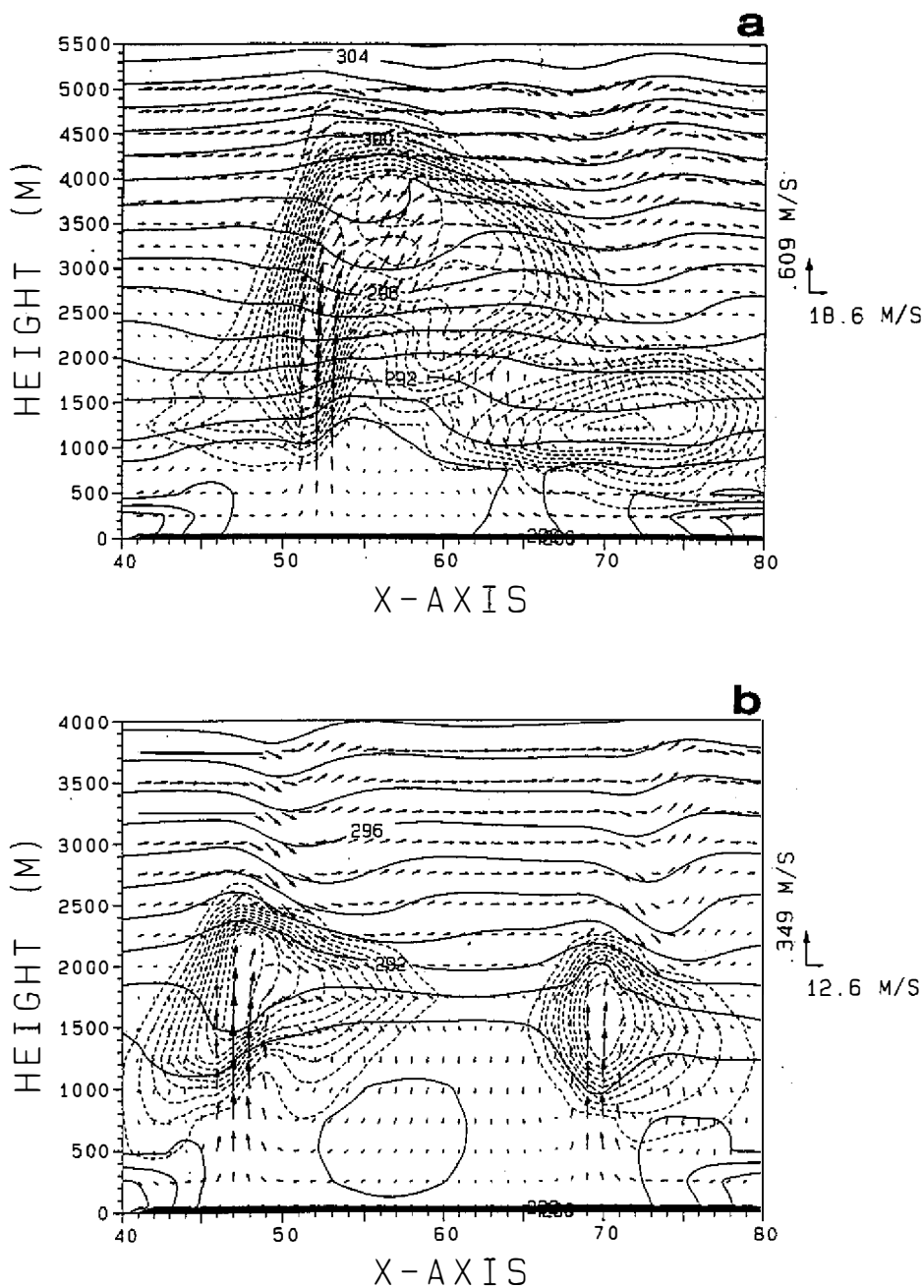
Fig. 5. Selected flow regimes over the Taiwan Strait at 24 h. (a) Case 2 (with RH of 80%) and (b) Case 3 (with RH of 50%). The three contour indices (minimum, maximum, interval) in units of 0.01 g kg^{-1} for cloud water (dashed lines) are (5, 65, 5) in (a) and (5, 55, 5) in (b).
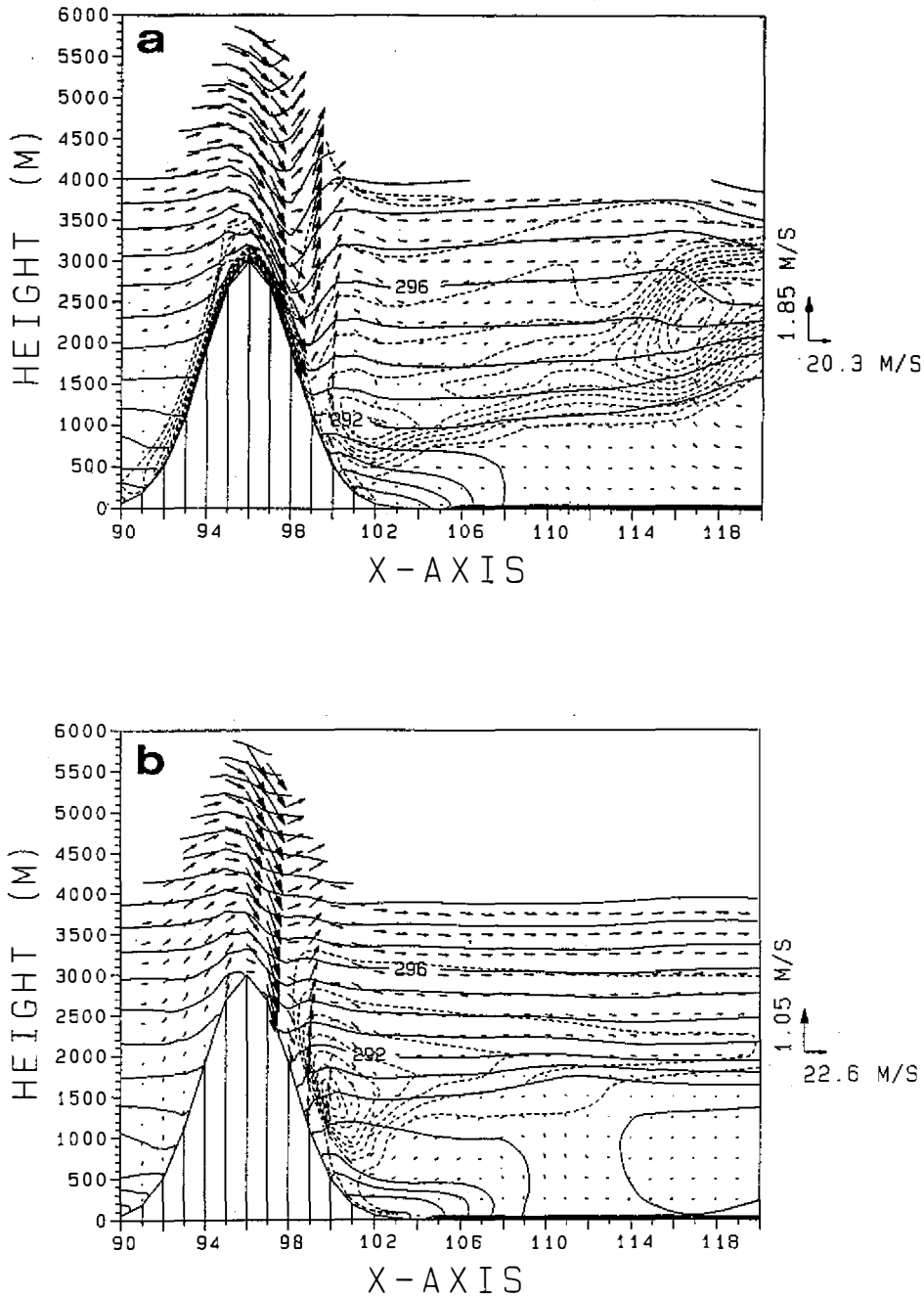
Fig. 6. Selected flow regimes east of the CMR at 24 h. (a) Case 2 and (b) Case 3. The three contour indices (minimum, maximum, interval) in units of 0.01 g kg^{-1} for cloud water (dashed lines) are (5, 60, 5) in (a) and (5, 45, 5) in (b).
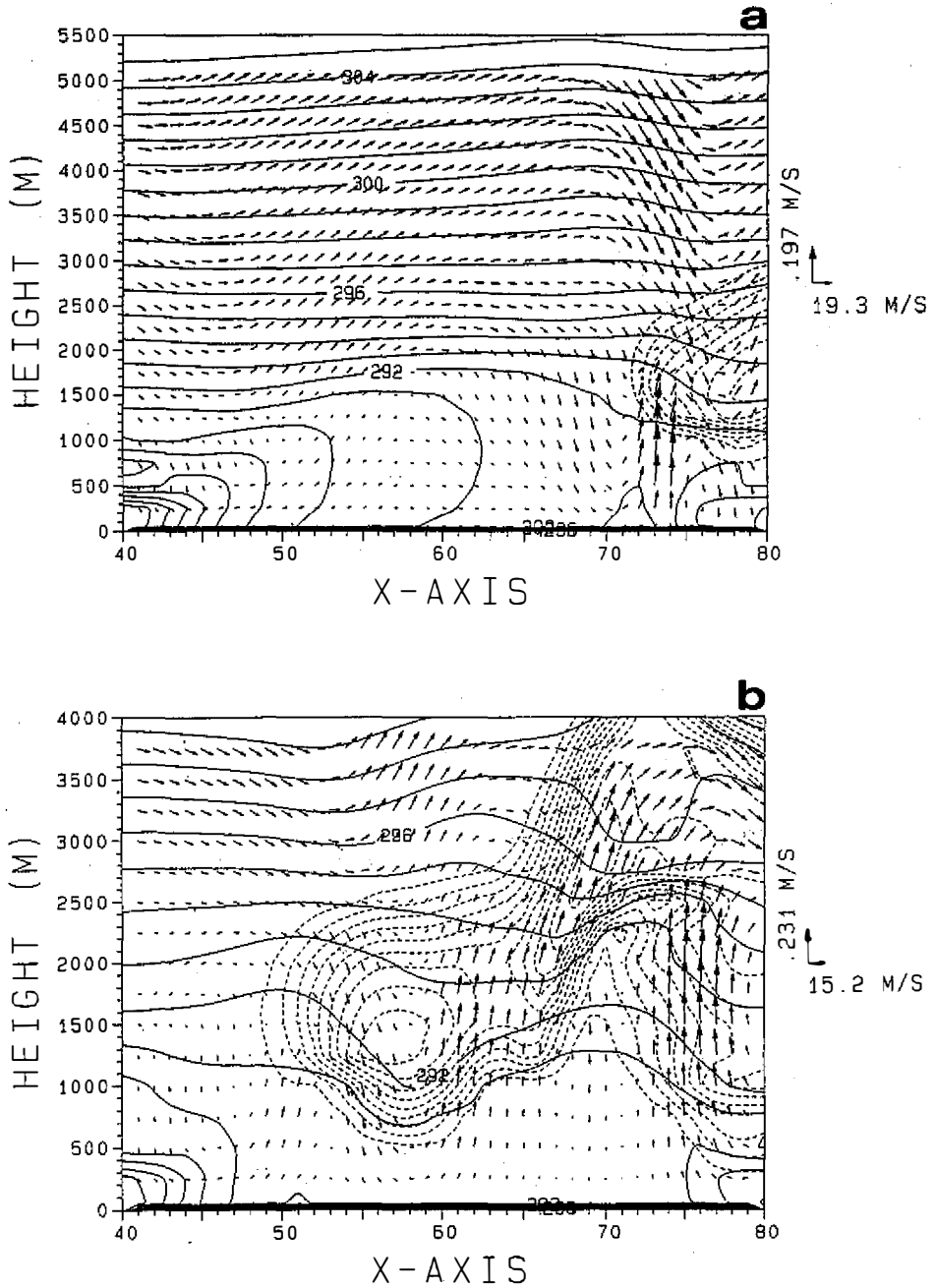
Fig. 7. Selected flow regimes over the Taiwan Strait at 36 h. (a) Case 2 and (b) Case 3. The three contour indices (minimum, maximum, interval) in units of 0.01 g kg^{-1} for cloud water (dashed lines) are (5, 40, 5) in (a) and (5, 60, 5) in (b).

by Huang and Raman (1992). The development of the two land breezes in the Taiwan Island is also intimately related to this same frontogenesis. The difference between the coastal front and the breeze front in the model results is the intensity and coverage area of cold air masses. Coastal fronts are known to be associated with cold air damming over the ground. The land breezes in our cases are driven by the effects of non-diurnal differential heating over the ocean and the land, and they should be distinguished from the daily land breeze in which the nighttime radiation cooling over land is responsible for an offshore wind development. Convective MBL is generated over the entire ocean for the former but for the latter only near the shorter water fetches where the breeze circulation develops.

Coastal frontogenesis is commonly seen in the eastern and southeastern U.S. coasts during the winter. In a climatological study, Bosart (1975) suggested that the New England frontogenesis is a result of boundary-layer frictional deformation. This boundary-layer induced circulation, more precisely, is related to ocean heating in the Presidents' Day Snowstorm event (Bosart, 1981). Although a coastal frontal circulation is a thermally direct circulation, coastal frontal formation was not well documented in the literature for the southeastern China coastal region in the winter and late spring. This may be due to the relatively lower position of the subtropical high-pressure system that provides the larger along-coast wind component as the southwest Asian monsoon shows. The large-scale flow pattern hence is not favorable for intense coastal frontogenesis at most times. For this case, geostrophic deformation may be the dominant mechanism for the frontogenesis along the coast. As the subtropical high moves to lower latitudes and westward, the onshore component of the large-scale ambient flow will increase and may imply a more favorable environment for coastal frontogenesis. Based on the results shown above, it can be seen that the modeled coastal front has structural similarities with low-level parts of Mei-Yu fronts in the vicinity of the southeastern China coast (*e.g.*, Chen and Hui, 1990), indicating that differential heating plays a similar role as the geostrophic deformation in frontogenesis.

The assumption of two-dimensionality in the model has greatly reduced the application ranges of the case results. This is mainly due to the limited length of Taiwan Island and the CMR. Also, the long-ridge type of terrain should have a length scale several times greater than the Rossby deformation radius (Nh/f) of the flow in order to minimize the influence of the surrounding flow on the directing flow. In reality, the elongated CMR with varied elevation heights does not have the modeling property of two-dimensionality for a uniform flow with the Rossby deformation radius of about 400 km as in our cases. The previous discussions on the influences of the topographic effects on the front thus were appropriate only for a small portion of the frontal cloud bands that interacts with the topography.

5. CONCLUSION

In this study, a two-dimensional mesoscale numerical model is used to investigate topographic influences on shallow front formation and evolution. Local topographic features include Taiwan Strait, the Taiwan Island and the Central Mountain Range (CMR). The shallow front is idealized as a coastal front near the southeastern China coast. As found, shallow coastal frontogenesis over the China coast is a direct result of differential boundary layer development for near-surface onshore ambient flow. The idealized shallow coastal front shows similar thermal structures with the lower part of Mei-Yu fronts stagnating over the southeastern China coast (Chen *et al.*, 1989), indicating that differential heating for the former similarly plays the role of geostrophic deformation in frontogenesis for the latter. Although

the packed frontal isentropes tend to reside over the China coast, the frontal leading updraft may advect offshore as the shear of the upper-level offshore ambient flow is present.

With numerical control experiments, topographic effects on the frontal evolution are investigated. It was found that the combined effects of the land breeze resistance and the CMR blocking could greatly enhance the cloud development during the eastward movement of the frontal updraft. The confrontation of the approaching frontal flow with the land breeze is an important factor for cloud formation over the coastal region. Cloud formation is apparently strong over the CMR due to orographic lifting. The enhancement of cloud development also depends on the availability of the ambient moisture over the boundary layer.

The numerical study provides an understanding of the processes in the shallow coastal frontogenesis and the interaction processes among the front, the land breeze and the down-stream orography. The coastal frontal cloud band may migrate offshore or remain near-stationary, depending on the intensity of the near-surface onshore ambient flow, the shear structure and the variation of the continental cold air intensity. We have presented the case results of quasi-stationary shallow fronts in this study. The case results of offshore migrating fronts will be presented in another paper.

REFERENCES

Bosart, L. F., 1975: New England coastal frontogenesis. *Quart. J. Roy. Meteor. Soc.*, **98**, 735-744.

Bosart, L. F., 1981: The Presidents' Day Snowstorm of 18-19 February 1979: A subsynoptic-scale event. *Mon. Wea. Rev.*, **109**, 1542-1566.

Chen, Y.-L., Y.-X. Zhang, and N. B.-F. Hui, 1989: Analysis of a surface front during the early summer rainy season over Taiwan. *Mon. Wea. Rev.*, **117**, 909-932.

Chen, Y.-L., and N. B.-F. Hui, 1990: Analysis of a shallow front during the Taiwan Area Mesoscale Experiment. *Mon. Wea. Rev.*, **118**, 2649-2667.

Hoskins, B. J., and F. P. Bretherton, 1972: Atmospheric frontogenesis models: Mathematical formulation and solution. *J. Atmos. Sci.*, **29**, 11-37.

Huang, C. Y., and S. Raman, 1991a: Numerical simulation of January 28 cold air outbreak during GALE. Part I: The model and sensitivity tests of turbulence closures. *Bound.-Layer Meteor.*, **55**, 381-407.

Huang, C. Y., and S. Raman, 1991b: A comparative study of numerical advection schemes featuring a one-step modified WKL algorithm. *Mon. Wea. Rev.*, **119**, 2900-2918.

Huang, C. Y., and S. Raman, 1992: A three-dimensional numerical investigation of a Carolina coastal front and the Gulf Stream rainband. *J. Atmos. Sci.*, **49**, 560-584.

Tang, T.-Y., and J.-Y. Chen, 1990: CTD data bank, Volume II, proposal report of National Science Council in R.O.C., NSC78-0206-P002a-04, 224 pp.